Neuroscience 278 (2014) 237–252

DISTRIBUTION OF GLIAL CELLS IN THE AUDITORY BRAINSTEM: NORMAL DEVELOPMENT AND EFFECTS OF UNILATERAL LESION

M. L. DINH, S. J. KOPPEL, M. J. KORN AND K. S. CRAMER*

Department of Neurobiology and Behavior, University of California Irvine, Irvine, CA 92697-4550, United States

Abstract—Auditory brainstem networks facilitate sound source localization through binaural integration. A key component of this circuitry is the projection from the ventral cochlear nucleus (VCN) to the medial nucleus of the trapezoid body (MNTB), a relay nucleus that provides inhibition to the superior olivary complex. This strictly contralateral projection terminates in the large calyx of Held synapse. The formation of this pathway requires spatiotemporal coordination of cues that promote cell maturation, axon growth, and synaptogenesis. Here we have examined the emergence of distinct classes of glial cells, which are known to function in development and in response to injury. Immunofluorescence for several astrocyte markers revealed unique expression patterns. Aldehyde dehydrogenase 1 family member L1 (ALDH1L1) was expressed earliest in both nuclei, followed by S100ß, during the first postnatal week. Glial fibrillary acidic protein (GFAP) expression was seen in the second postnatal week. GFAP-positive cell bodies remained outside the boundaries of VCN and MNTB, with a limited number of labeled fibers penetrating into the margins of the nuclei. Oligodendrocyte transcription factor 2 (OLIG2) expression revealed the presence of oligodendrocytes in VCN and MNTB from birth until after hearing onset. In addition, ionized calcium binding adaptor molecule 1 (IBA1)-positive microglia were observed after the first postnatal week. Following hearing onset, all glial populations were found in MNTB. We then determined the distribution of glial cells following early (P2) unilateral cochlear removal, which results in formation of ectopic projections from the intact VCN to ipsilateral MNTB. We found that following perturbation, astrocytic markers showed expression near the ectopic ipsilateral calyx. Taken together, the developmental expression patterns are consistent with a role for glial cells in the maturation of the calyx of Held and suggest that these cells may have a similar role in maturation of lesion-induced connections.

Key words: deafferentation, brainstem, auditory system, astrocyte, microglia, oligodendrocyte.

INTRODUCTION

Precise neural circuits in the auditory brainstem compute binaural timing and intensity disparities that are used to localize sound sources. In mammals, auditory information is carried by the VIIIth cranial nerve into the central nervous system (CNS), where branches of VIIIth nerve fibers terminate onto targets in the ventral cochlear nucleus (VCN). VCN globular bushy cells project to the contralateral medial nucleus of the trapezoid body (MNTB) where their large reticulated terminations, the calyces of Held, synapse onto principal neurons (Kuwabara and Zook, 1991; Kuwabara et al., 1991; Kandler and Friauf, 1993; Kil et al., 1995). MNTB neurons in turn provide glycinergic inhibition to the medial superior olive (MSO) and the lateral superior olive (LSO), which integrate excitation and inhibition to compute interaural time differences and interaural level differences, respectively.

This unique projection matures over a protracted period of development (Nakamura and Cramer, 2011). Axons reach contralateral MNTB and form immature connections by embryonic day (E) 17 (Borst and Soria van Hoeve, 2012). At postnatal day (P) 0, rudimentary calyces are seen with several inputs on each MNTB neuron. As the terminations expand, the number of VCN inputs is reduced until a single input encapsulates each MNTB neuron by P4 (Hoffpauir et al., 2006; Holcomb et al., 2013). Synapse formation and pruning have been shown to involve several forms of cell–cell communication. Notably, glial-secreted factors play a role in synaptic maturation (Mauch et al., 2001; Christopherson et al., 2005; Hughes et al., 2010; Kucukdereli et al., 2011; Allen et al., 2012; Korn et al., 2012). In addition, several types of glial cells have been shown to be important for synaptic refinement both in development and in response to injury (Chung and Barres, 2012; Karimi-Abdolrezaee and Billakanti, 2012; Schafer et al., 2012; Wake et al., 2013).

While the contribution of glial cells to the maturation of the central auditory circuitry is not known, recent studies have reported that astrocytes contact both the pre- and

*Corresponding author. Tel: +1-949-824-4211; fax: +1-949-824-2447.
E-mail address: cramerk@uci.edu (K. S. Cramer).

Abbreviations: aCSF, artificial cerebrospinal fluid; ALDH1L1, aldehyde dehydrogenase 1 family member L1; CR, cochlear removal; DAPI, 4′,6-diamidino-2-phenylindole; DCN, dorsal cochlear nucleus; GFAP, glial fibrillary acidic protein; HEPES, 4-(2-hydroxyethyl)-1-piperazineethanesulfonic acid; IBA1, ionized calcium binding adaptor molecule 1; MNTB, medial nucleus of the trapezoid body; OLIG2, oligodendrocyte transcription factor 2; PBS, phosphate-buffered saline; PFA, paraformaldehyde; RDA, rhodamine dextran amine; SEM, standard error of the mean; VCN, ventral cochlear nucleus.

http://dx.doi.org/10.1016/j.neuroscience.2014.08.016
0306-4522/

postsynaptic membranes of the calyx of Held (Elezgarai et al., 2001). These astrocytes elicit slow inward currents in the postsynaptic MNTB neuron via gliotransmission in the mature animal (Reyes-Haro et al., 2010). The close apposition of astrocytes to the calyx suggests a potential role for astrocytes in the development and function of this pathway.

To explore the role(s) of glial cells in the maturation of auditory circuits, we characterized the spatiotemporal emergence of glial subtypes in the VCN and MNTB. We used several markers to identify multiple astrocyte-specific proteins, including the intermediate filament glial fibrillary acidic protein (GFAP), the calcium binding protein S100β, and aldehyde dehydrogenase 1 family member L1 (ALDH1L1) (Cahoy et al., 2008). Oligodendrocytes were identified by expression of oligodendrocyte transcription factor 2 (OLIG2). The emergence of microglia was assessed by expression of the ionized calcium binding adaptor molecule 1 (IBA1).

Additional clues to mechanisms of neural circuit formation may be obtained from experimentally induced reorganization of synapses. Following early postnatal unilateral cochlear removal, the cochlear nucleus on the deafferented side undergoes substantial cell death (Trune, 1982; Hashisaki and Rubel, 1989; Mostafapour et al., 2000). Axons from the intact VCN subsequently branch and contact the ipsilateral, denervated MNTB, in addition to their normal contralateral target (Moore and Kowalchuk, 1988; Kitzes et al., 1995; Hsieh and Cramer, 2006; Hsieh et al., 2007). Here we examined the expression of glial markers in denervated and intact MNTB after cochlear removal.

During normal development we found a diversity of patterns for development of glial cell types in VCN and MNTB from birth to the time of hearing onset. We found that expression of astrocyte and oligodendrocyte markers following cochlear removal was similar to the distribution of these glial markers during normal development. In addition, glial cells and their processes were seen in close proximity to the emerging ipsilateral calyx; as in normal development, these populations were primarily astrocytes. Together with our developmental expression data, we posit that glial cells may be important for the development and early plasticity of the mammalian auditory circuit, and that different glial cell types may serve distinct functions in this pathway.

EXPERIMENTAL PROCEDURES

Animals

Wild-type mice on CD-1 background were used for these studies. Expression studies included animals at several developmental ages, including postnatal day (P)0 (n = 6); P6 (n = 9); P14 (n = 10); and P23 (n = 7). Cochlear removal (CR) or sham operation was performed at P2 and animals survived until P4 (n = 9 for CR and n = 9 for sham) or P9 (17 CR and 11 sham). All procedures were approved by the University of California, Irvine Institutional Animal Care and Use Committee.

Immunohistochemistry

Pups were euthanized with isoflurane and perfused with 0.9% saline in phosphate-buffered saline (PBS) followed by 4% paraformaldehyde (PFA). Brainstems were fixed for 2 h in PFA and cryoprotected in 30% sucrose in PBS overnight at 4 °C. Tissue was sectioned coronally on a cryostat (Leica Microsystems, Buffalo Grove, IL, USA) at 18–20 μm thickness onto chrome-alum-coated slides. Sections were outlined in PAP pen (Binding Site, San Diego, CA, USA) to provide a hydrophobic layer and heated on a slide warmer at 37 °C for 30 min. Slides were rinsed in PBS and blocked with 4% bovine serum albumin (BSA) in 0.1% Triton-X100 in PBS for 1 h at room temperature. Slides were incubated in primary antibodies diluted in blocking solution overnight at room temperature in a humid chamber. The following day, slides were rinsed with PBS and incubated with goat anti-rabbit, goat anti-mouse, or donkey anti-chicken secondary antibody (1:300, Alexa Fluor, Invitrogen, Carlsbad, CA, USA) at room temperature for 1 h. Slides were then rinsed with PBS and cover slipped with Prolong Gold Anti-Fade mounting medium with 4′,6-diamidino-2-phenylindole (DAPI) to label cell nuclei (Invitrogen).

Antibodies

For immunofluorescence we used primary antibodies to identify five different glial markers for astrocytes, oligodendrocytes and microglia. For astrocytes, we used three antibodies: S100β, GFAP, and ALDH1L1. Rabbit S100β (1:500, Abcam, Cambridge, MA, USA) is a monoclonal antibody generated from a synthetic peptide corresponding to C-terminus human S100β. S100β is an 11-kDa calcium binding protein found in mature CNS astrocytes. Anti-GFAP chicken polyclonal antibody (1:1000, Abcam) was generated against the full length native bovine protein (50 kDa). GFAP antibody was purified from a Triton-X100 extract of myelin-associated material, and purified by centrifugation and ion exchange chromatography. The GFAP antibody stains for both reactive and resting state astrocytes. Anti-ALDH1L1 rabbit polyclonal antibody (1:500, Abcam), was generated from a synthetic peptide conjugated to KLH derived from a peptide sequence within amino acid residues 300–400 of mouse ALDH1L1. Anti-OLIG2 was used as an oligodendrocyte-specific marker (1:500, Millipore, Temecula, CA, USA). The polyclonal rabbit antibody was generated against the recombinant mouse OLIG2. Microglia-specific populations were stained using rabbit anti-IBA1 polyclonal antibody (1:1000, Wako). The antibody was generated from a synthetic peptide (PTGPPAKKAISELP) corresponding to the C-terminus fraction of the protein and purified by antigen affinity chromatography from rabbit antisera.

Cochlear removal

CR was performed at P2 using previously published methods (Hsieh and Cramer, 2006; Hsieh et al., 2007; Nakamura and Cramer, 2011). Animals were

anesthetized with hypothermia and a small incision was made ventral to the pinna to expose the tympanic membrane. A sterile glass pipette was used to aspirate out the cochlea. In sham-operated animals, all procedures were performed except the aspiration. Surgery was performed under a stereomicroscope with heat-sterilized instruments (Germinator 500, Cell Point Scientific, Gaithersburg, Maryland, USA). After surgery, pups were returned to their mother and allowed to recover two or seven days before perfusion. Flunixin, a local analgesic, was administered at 2.5 mg/kg for two days, beginning with the day of surgery. Pups were used for both neuroanatomical labeling of VCN–MNTB projections and expression of glial markers following lesion. The efficiency of CR was evaluated by a decrease in size of deafferented VCN together with neuronal tracing to visualize ipsilateral VCN–MNTB projections.

Neuroanatomical labeling

Axonal projections from VCN to MNTB were visualized using rhodamine dextran amine (RDA, MW: 3000, Invitrogen) dye injections. The injection solution included 6.35% RDA with 0.4% Triton-X100 in PBS. Brainstems were isolated and submerged in artificial cerebrospinal fluid (aCSF; 130 mM NaCl, 3 mM KCl, 1.2 mM KH_2PO_4, 20 mM $NaHCO_3$, 3 mM HEPES, 10 mM glucose, 2 mM $CaCl_2$, 1.3 mM $MgSO_4$ perfused with 95% O_2 and 5% CO_2). A pulled glass micropipette was filled with RDA and pulses of RDA were injected medial to the cochlear nucleus using a Picospritzer at 25 ms. The region surrounding the injection site was electroporated at a rate of five pulses per second (pps) at 40 volts (V) for 50 milliseconds (ms). The tissue was immersed in aCSF for 2 h under continuous oxygenation to allow labeling of axonal projections, and then prepared for histological staining by fixation for two hours in PFA, rinsing, and incubation in 30% sucrose overnight.

Imaging

All images of glial cell types in VCN and MNTB were examined and analyzed using the Zeiss Axioskop microscope, Axiocam camera, and Axiovision software. High resolution images of calyces during development and after CR were acquired by a LSM 5 Pascal confocal microscope with a 63× oil objective. Images were imported into Adobe Photoshop to adjust brightness and contrast of the image collectively, and subsequently uploaded into Adobe Illustrator for further editing. We used DAPI nuclear labeling to assist in the identification of the cochlear nucleus and its subdivisions and MNTB.

Image analysis

Relative levels of expression of glial markers on the two sides of the brain were analyzed using either optical density measurements or cell counts. All analyses were performed blinded to the treatment group. MNTB was outlined using Zeiss Axioskop imaging software and optical density measurements were taken with average optical density subtracted by background intensity. For all animals, at least three sections per side were analyzed and values were averaged. To assess effects of unilateral CR, we obtained measurements from the MNTB contralateral to the lesion (the denervated MNTB) and from the MNTB ipsilateral to the lesion (the innervated MNTB). A ratio of these measurements, the denervated MNTB to innervated MNTB ratio (D/I ratio), was compared between CR animals and sham-operated controls. For IBA1, microglial cell density was determined by counting the number of immunopositive cells within MNTB and a D/I ratio similar to optical density measurements was used for comparisons. We quantified GFAP-positive processes using confocal images analyzed using a filament tracing program on the Imaris Software. Statistical comparisons were made with a nonparametric one-way ANOVA. Values reported in text are denoted as mean ± standard error of the mean (SEM).

To determine the extent to which glial cells surround or appose developing calyceal terminations, we analyzed images of RDA-labeled projections in CR animals. All of the labeled ipsilateral calyces were evaluated for immunofluorescent label in proximity to the calyx. We expressed a percentage of these calyces that had glial marker expression nearby. In each section examined, we also selected at least five labeled calyces on the normal, contralateral side using the red channel alone, then ascertained the percent of these calyces with apposing glial marker expression.

RESULTS

Expression of glial markers during the first postnatal week

As early as P0, glial markers were evident within the VCN, with notable variability in the expression of astrocyte proteins. GFAP at this age was sparse, limited to the ventral portion and in the central projection of the auditory nerve (Fig. 1A). ALDH1L1 (Fig. 1B) levels were abundant in the VCN, with less expression in the dorsal cochlear nucleus (DCN). S100ß displayed a pattern similar to that seen with GFAP (Fig. 1C).

The oligodendrocyte marker OLIG2 was expressed in the ventral portion of VCN and in the auditory nerve (Fig. 1D). IBA1 immunofluorescence revealed sparsely distributed microglial cells in the VCN (Fig. 1E). These microglia were ameboid in shape and exhibited few short processes consistent with active microglia (Fig. 1E′).

All astrocyte markers were expressed in the mouse auditory brainstem except GFAP, which was sparsely distributed along the ventral border of the brainstem, but was not found in MNTB (Fig. 2A). S100β was expressed in MNTB fibers to a limited extent, and did not share the ventral expression patterns seen with the other astrocyte markers (Fig. 2B). ALDH1L1 was distributed throughout the auditory level of the brainstem with strong expression at the ventral border with many fibrous processes labeled within MNTB (Fig. 2C, C′). The oligodendrocyte marker OLIG2 was sparsely along the ventral aspect of the brainstem with few cells inside MNTB (Fig. 2D). Staining for the microglial marker IBA1

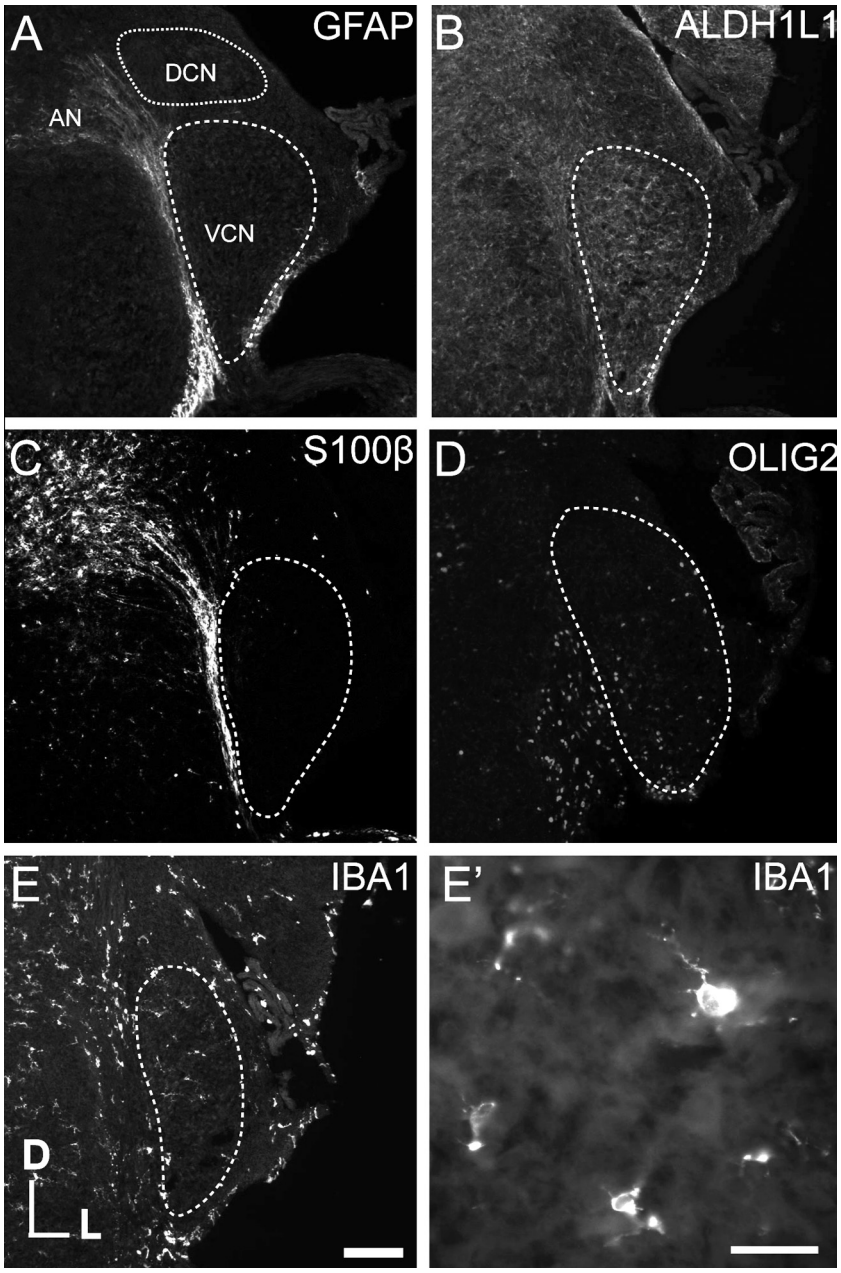

Fig. 1. Expression of glial markers in VCN at P0. (A) At P0, GFAP showed minimal expression in VCN but was evident in the adjacent central projection from the auditory nerve. (B) ALDH1L1 is expressed throughout VCN with less expression in DCN. (C) Similar to GFAP, S100β was expressed in the auditory nerve but excluded from VCN. (D) OLIG2 expression revealed limited cells along the ventral aspect of VCN and in the auditory nerve. (E and E′) IBA1 was expressed in a small number of cells in VCN that were mostly ameboid in shape with few processes (panel E′ another representative section). Scale bar in E = 100 μm, applies to Panels A–E. Scale bar in E′ = 50 μm.

showed characteristic microglial morphology with thin radial processes in a sparse distribution spread throughout the auditory level of the brainstem. While labeling in MNTB was minimal, the brainstem border ventral to MNTB showed high levels of expression of IBA1 (Fig. 2F).

By the end of the first postnatal week (P6), GFAP expression remained evident in the auditory nerve and low in VCN (Fig. 3A). ALDH1L1 and S100β showed similar expression patterns with fibrous processes in VCN. ALDH1L1 showed more limited expression in the auditory nerve compared to the other astrocyte markers (Fig. 3B, C). Compared to P0, there were many S100β-positive cells found surrounding globular bushy cells (Fig. 3C′). OLIG2-positive cells were observed in VCN, but few IBA1-positive cells were seen at this age (Fig. 3D, E). In comparison to P0, microglia at P6 had many complex processes with several radiating processes.

GFAP-positive fibers were present in the brainstem at P6, with significantly more processes within MNTB than at P0 ($p = 0.03$, Fig. 4A). ALDH1L1 and S100β-positive astrocytes were found throughout the MNTB nucleus (Fig. 4B, C), in contrast to the limited expression of

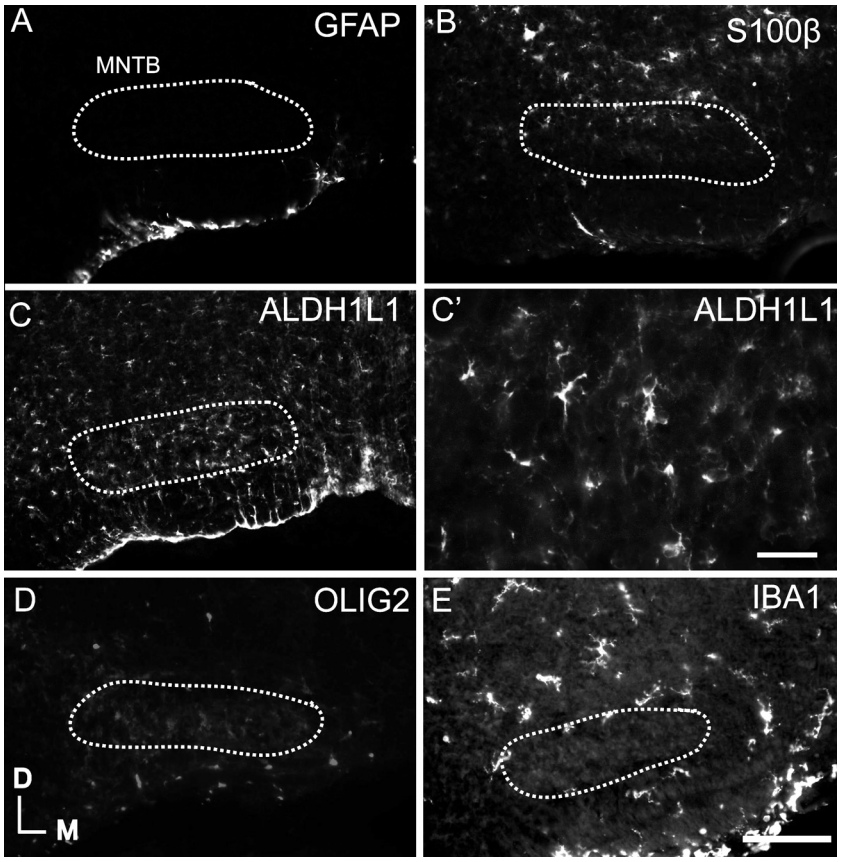

Fig. 2. Expression of glial markers in MNTB at P0. (A) GFAP expression was limited to the ventral portion of the brainstem outside MNTB. (B) S100β expression was minimal and limited to the dorsal region of MNTB. (C) ALDH1L1 was expressed by fibers surrounding MNTB principal neurons, and more generally throughout the brainstem. ALDH1L1 cells had several processes (C′). (D) OLIG2-positive cells were seen along the ventral brainstem. (E) IBA1-positive cells were found in brainstem, but not found in MNTB. Scale bar in E = 100 μm, applies to all panels except panel C′ (Scale bar = 50 μm).

GFAP. OLIG2 and IBA1 expression patterns showed more cells inside MNTB than at P0 (Fig. 4D, E). At this age, microglia had smaller cell bodies with more intricate processes (Fig. 4E′).

Expression of glial markers during the second and third postnatal weeks

We examined expression patterns of glial markers at P14, after hearing onset. By P14, all glial markers were expressed in VCN (Fig. 5). There was a significant increase in GFAP-positive fibers in VCN compared to P0 ($p < 0.05$), but in contrast to earlier ages, GFAP labeling was not observed in central auditory nerve fibers (Fig. 5A). S100β and ALDH1L1 continued to show expression in VCN, with diminished expression in the auditory nerve (Fig. 5C, D). Olig2 expression appeared throughout VCN (Fig. 5E). At this age VCN showed substantial expression of IBA1 (Fig. 5F).

Similar to VCN, MNTB showed an increase in the density of GFAP-positive fibers at P14 compared to P0 ($p < 0.001$, Fig. 6A, B). The expression patterns of S100β and ALDH1L1 in MNTB were similar to those observed at earlier ages (Fig. 6C, D). OLIG2 cells were found inside MNTB (Fig. 6E). At P14 numerous IBA1-positive fibers present within MNTB (Fig. 6F). Microglial processes at P14 were the most complex of all the ages analyzed, exhibiting many intricate, complex processes (Fig. 6F inset).

We next examined expression of glial markers in the auditory brainstem of animals at P23, when the auditory brainstem pathways are mature. GFAP expression was upregulated at this age compared to prior time points with several cell processes within VCN (Fig. 7A–A′). The expression of ALDH1L1 and S100β within VCN appeared to decrease by P23 (Fig. 7B, C). OLIG2-positive cells remained prominent throughout VCN (Fig. 7E). IBA1 expression was sparsely distributed at P23 (Fig. 7F).

GFAP-positive fibers remain numerous in MNTB, albeit expression levels were decreased compared to P14 ($p = 0.02$, Fig. 8A). S100β showed an expression profile similar to earlier time points (Fig. 8B). ALDH1L1 expression was high in MNTB and showed dense labeling around principal neurons rather than the fibrous labeling seen at earlier ages (Fig. 8C–C′). OLIG2 expression showed cells predominantly located along the ventral portion of MNTB (Fig. 8D). IBA1 expression remained in MNTB, although it appeared reduced relative to that seen at P14. IBA1-positive cells at P23

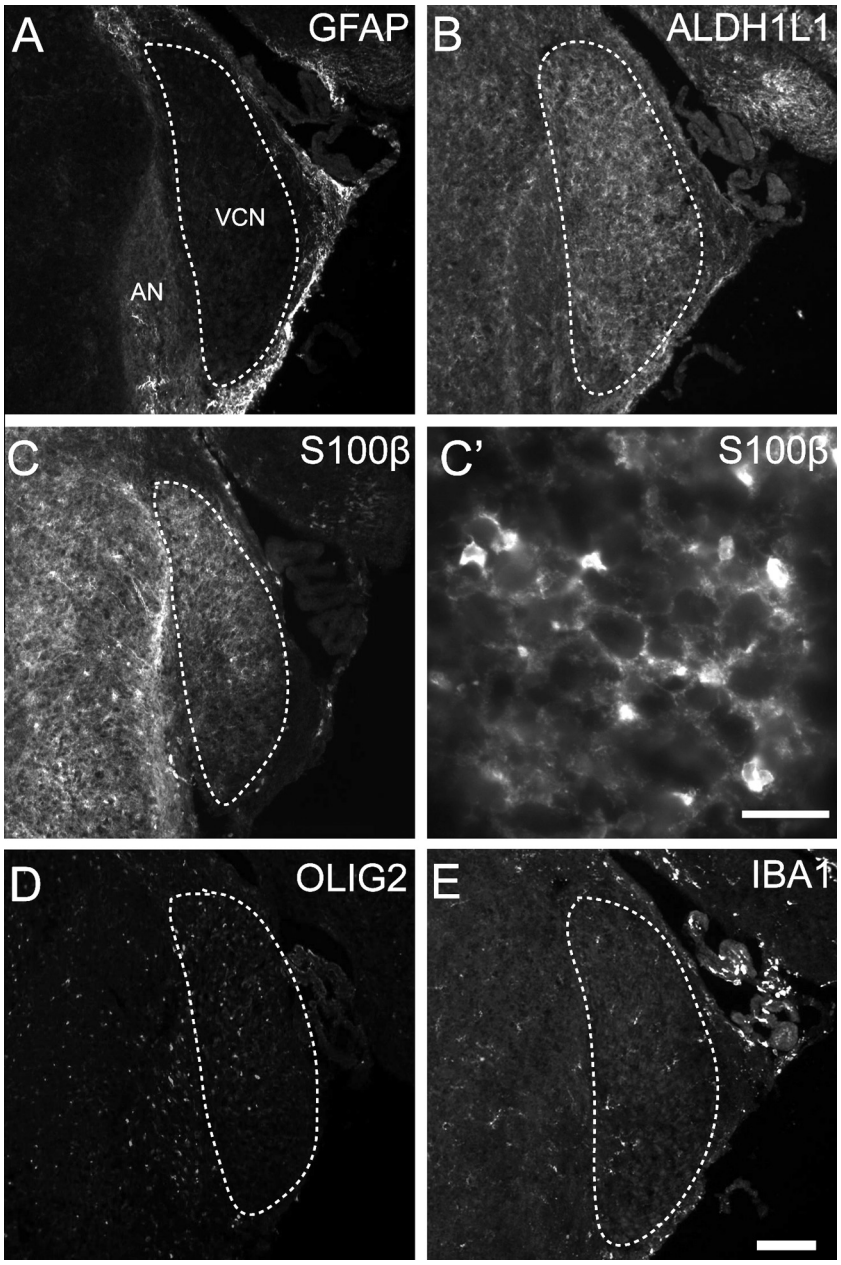

Fig. 3. Expression of glial markers in VCN at P6. (A) Similar to P0, GFAP expression is limited to the auditory nerve. (B–C) ALDH1L1 and S100β have similar expression patterns in VCN, including the presence of immunopositive fibrous processes. S100β-positive cells are seen in auditory nerve and in VCN encapsulating the globular bushy cells (C′). (D) OLIG2-positive cells were seen throughout VCN. (E) Few IBA1-positive cells could be observed throughout the VCN. Scale bar in F = 100 μm, applies to all panels except C′ (Scale bar = 50 μm).

were also smaller in size compared to the ameboid cells observed at P0 (Fig. 8E).

Glial subtypes apposed to the developing calyx

To investigate the extent to which glial cells associate with the developing calyx of Held, we traced VCN–MNTB projections with RDA unilaterally and stained for glial markers (Fig. 9). At P6, the calyx is maturing and elaborating its morphological structure, while additional inputs to MNTB neurons are being eliminated (Holcomb et al., 2013). Both ALDH1L1 and S100β-positive astrocytes were found within the MNTB region in between principal neurons, often adjacent to labeled calyces (Fig. 9A, B). No GFAP processes were found adjacent to developing synapses, consistent with the paucity of GFAP-positive fibers at this age (Fig. 9C). Microglia were distributed sparsely across MNTB, often nearby developing calyces (Fig. 9D). In relation to the calyx, some OLIG2-positive cells were located near the principal neuron, occasionally overlapping with the developing calyx (Fig. 9E).

We next examined the association between glial cells in MNTB and the relatively mature calyx after hearing onset at P14 (Fig. 9). ALDH1L1-positive astrocytes were closely aligned along the contours of MNTB principal

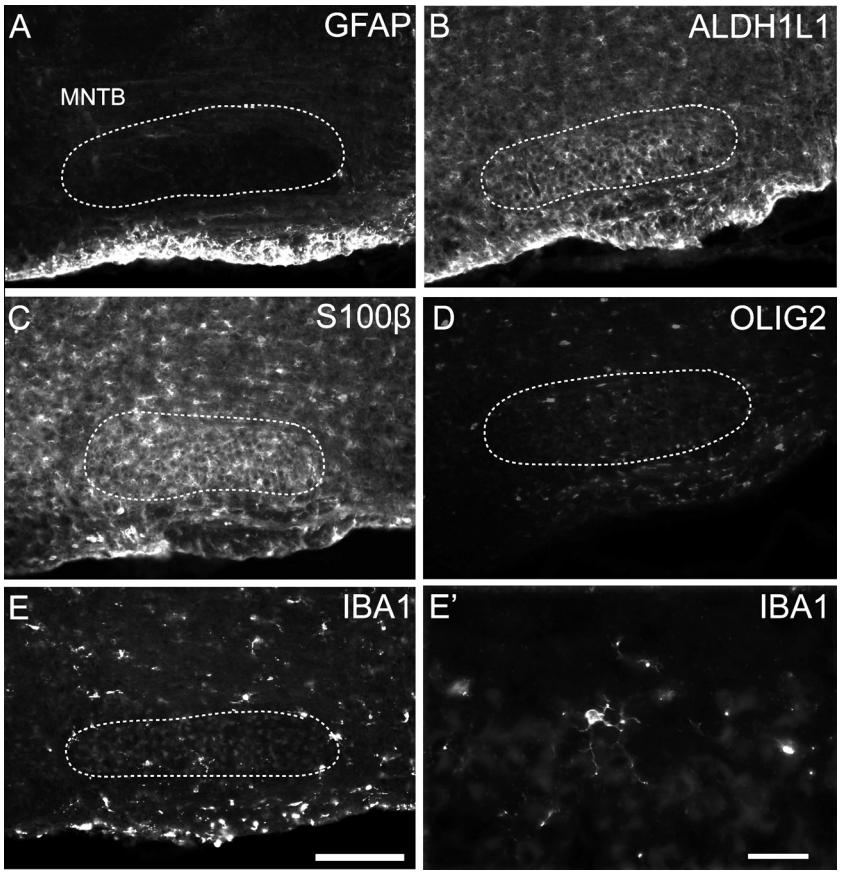

Fig. 4. Expression of glial markers in MNTB at P6. (A) While all other astrocytic markers were present throughout brainstem, GFAP expression was limited to fibers in the ventral region of brainstem with more processes in MNTB than at younger age (GFAP at P6 was 595.54 ± 70.14 was significantly higher than GFAP at P0 (143.12 ± 68.79, $p = 0.03$). (B–C) Expression of ALDH1L1 and S100β revealed processes throughout MNTB. (D) OLIG2 immunofluorescence was seen in spherical cells within MNTB. (E) IBA1-positive cells were found throughout the brainstem, particularly at the ventral margin. IBA1-positive cells in MNTB mostly had small cell bodies with elongated processes (E′). Scale bar in F = 100 μm, applies to panels A–E. Scale bar in E′ = 50 μm.

neurons, often situated in apposition to the calyx (Fig. 9F), filling in spaces not occupied by the terminal. S100β-positive astrocytes showed an even distribution across MNTB, and were interleaved on the postsynaptic cell not taken up by the calyx (Fig. 9G). At this age, GFAP-positive astrocytes were found in MNTB, with astrocytic processes present near calyces (Fig. 9H). Microglia were distributed throughout MNTB at this age, with occasional fibers in the vicinity of calyceal endings (Fig. 9I). Oligodendrocyte staining revealed a similar expression pattern to younger ages, with OLIG2-positive cells near the MNTB neurons (Fig. 9J).

Expression of glial proteins in MNTB following unilateral cochlear lesion

The dynamic expression patterns of astrocyte and microglial cell populations during formation of auditory system connections prompted us to assess how these populations respond during deafferentation-induced formation of new connections. We performed unilateral cochlear ablation to induce ipsilateral sprouting. Tissue was collected at two time points after surgery, P4 and P9, and we performed subsequent immunofluorescence and dextran dye labeling to assess expression of glial markers during the maturation of the newly formed calyx (Fig. 10).

We observed ALDH1L1-positive astrocytes positioned closely to the majority of normal, contralateral calyces (95%) and lesion-induced ipsilateral calyces (94%; Fig. 10A). Similarly, S100β-positive astrocytes surrounded the new calyx with several processes invading the postsynaptic space (Fig. 10B). S100β-positive astrocytes were observed in proximity to 94% of normal contralateral calyces and 96% of induced ipsilateral calyces. In addition, GFAP-positive processes coursed throughout the MNTB, with some processes along the newly formed calyx (74%, Fig. 10C). In contrast to the astrocyte labeling, microglial staining showed minimal microglia near the ectopic calyx, in which only half of the calyces had apposition of IBA1-positive expression (Fig. 10D). Lastly, staining for oligodendrocytes revealed a similar expression pattern to normal development, in which OLIG2-positive staining were minimally expressed around postsynaptic cells in MNTB – in this case, less than half of the calyces observed had oligodendrocyte apposition (Fig. 10E).

We quantitatively assessed the density of glial cells using optical density for all markers except IBA1, for which we used cell counts, and GFAP, for which we

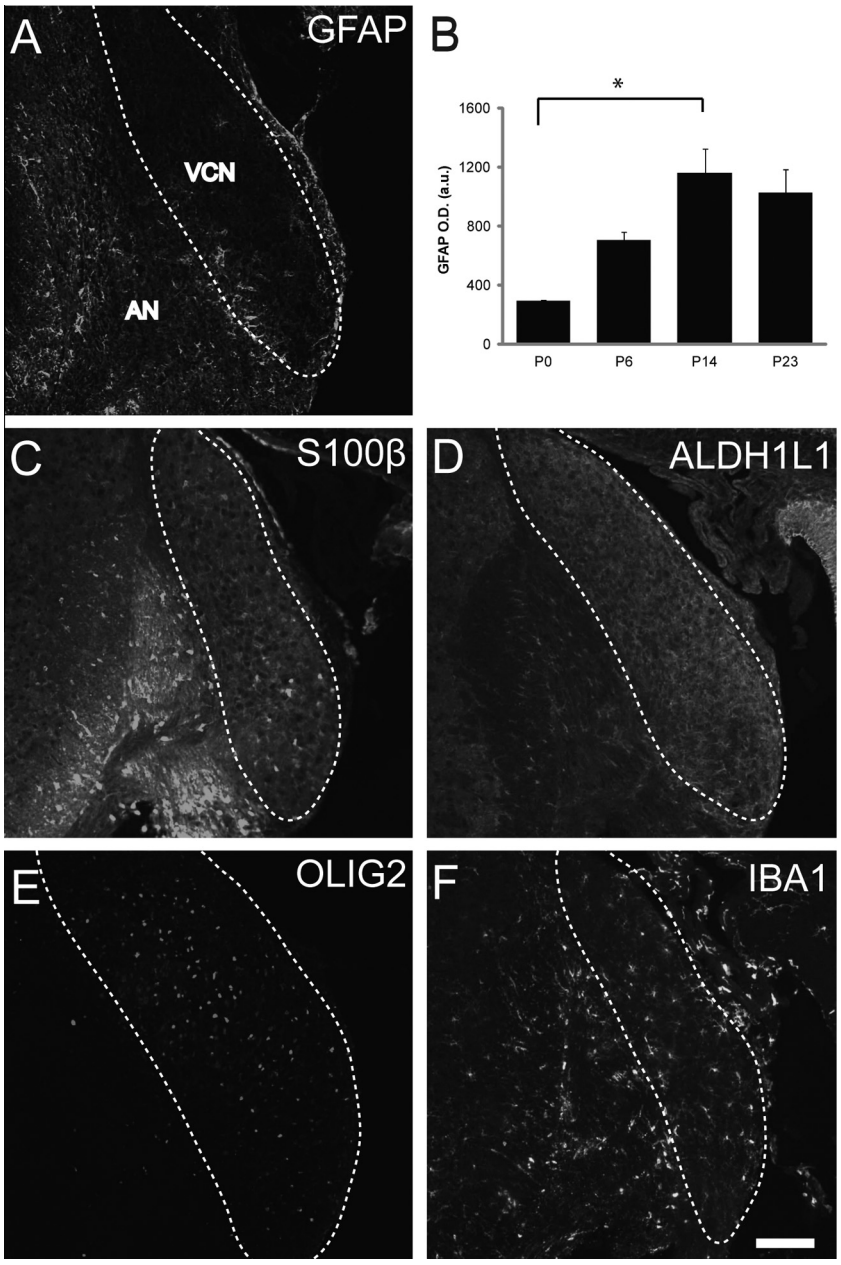

Fig. 5. Expression of glial markers in VCN at P14. (A) At P14, an increase in GFAP-positive fibers was seen in VCN in comparison to earlier ages ($p = 0.05$; the GFAP O.D. at P0 was 294.74 ± 3.41 while the GFAP O.D. at P14 was 1158.50 ± 165.08). (B–E) Astrocytic markers GLAST, S100β and ALDH1L1 were all expressed in VCN. (E) Cellular OLIG3 expression was seen throughout VCN. (F) Several IBA1 expressing cells could be identified within VCN. Scale bar in F = 100 μm, applies to all panels.

measured total process length. For each of the measures we computed a ratio, the D/I ratio, which was compared to similar counts in unilaterally sham-operated animals. Analysis revealed that after a two-day survival period, these ratios were not significantly different (ANOVA, $p = 0.23$, Fig. 11, panel A–E). Similarly, D/I ratios did not differ between CR and sham controls after seven days post-operative (ANOVA, $p = 0.13$, Fig. 11, panel F–J).

DISCUSSION

We have characterized the developmental emergence of distinct glial populations in the auditory brainstem, focusing on the projection from VCN to MNTB in relation to the developing calyx of Held. Additionally, we performed similar studies on lesion-induced ipsilateral projections. These studies provide clues to the function of glial cells in auditory synaptogenesis, and suggest that induced calyces share similar glial involvement with normal contralateral calyces.

Glial distribution in brainstem postnatal development – connection to developmental events

In this study we explored the developmental expression pattern of several glial markers in the mouse auditory brainstem during normal postnatal development and

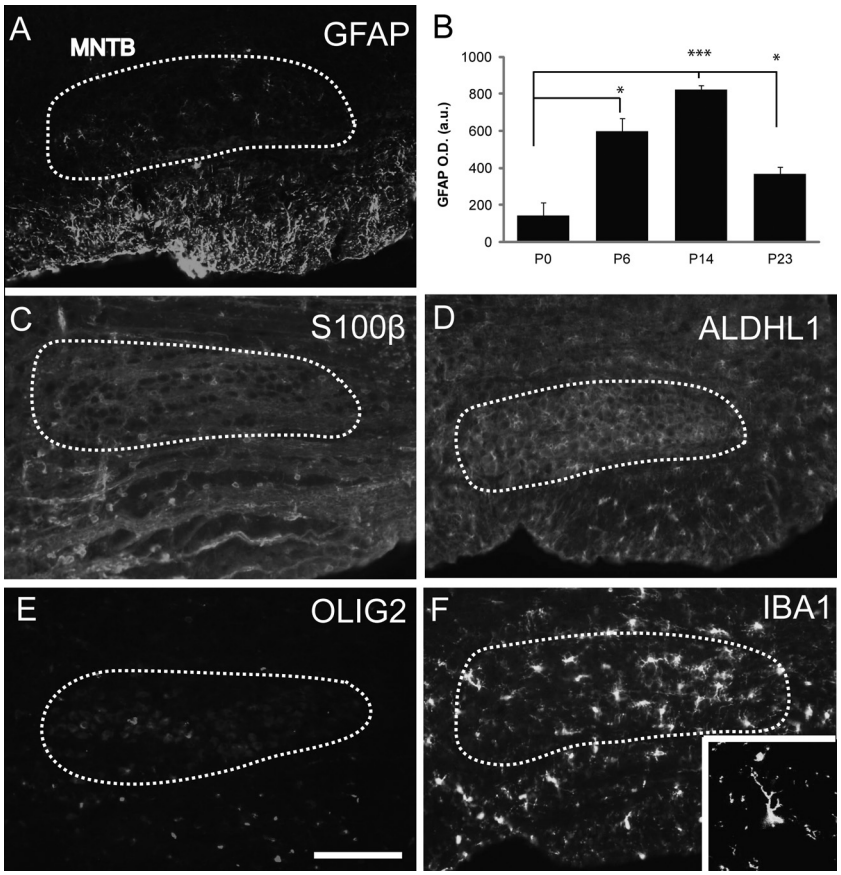

Fig. 6. Expression of glial markers in MNTB at P14. (A and B) GFAP-positive fibers were observed penetrating MNTB from the ventral boundary and was significantly increased compared to P0 ($p = 0.001$; GFAP at P14 was 821.08 ± 23.11 compared to GFAP at P0 (143.12 ± 68.79). (C–D) Similar to younger ages, S100β and ALDH1L1 were expressed throughout the brainstem and inside MNTB, surrounding principal neurons. (E) OLIG2 expression showed few cells in MNTB. (F) IBA1 expression had cell bodies penetrating MNTB with many cells possessing intricate processes (inset). Scale bar in F = 100 μm, applies to all panels.

following early unilateral CR. To explore the role of glial cells in the establishment of auditory connections, we examined the expression of glial markers during maturation of the auditory pathway (Borst and Soria van Hoeve, 2012). At P0, VCN axons in MNTB synapse onto multiple postsynaptic targets through collateral branches (Rodriguez-Contreras et al., 2008). We found distinct temporal expression profiles of astrocytes, oligodendrocytes, and microglia. GFAP and S100β expression appeared at low levels beginning at P0 along the ventral border of the brainstem and VCN, with high expression in the auditory nerve. Expression was robust for ALDH1L1 in VCN and MNTB. Like GFAP-positive astrocytes, IBA1-positive microglia were present sparsely in VCN, but not in MNTB. OLIG2 expression revealed minimal labeling in VCN and MNTB, with many cells located in the auditory nerve. At P6, an early protocalyx has formed and collaterals are extensively pruned so that each MNTB principal neuron receives a single calyceal input (Rodriguez-Contreras et al., 2008). With the exception of GFAP, all astrocytic markers screened were expressed in VCN and MNTB at this age. Few IBA1-positive cells were seen in VCN and MNTB at P6. OLIG2-positive cells were distributed throughout VCN and in MNTB.

We examined glial marker expression at P14, after the period of hearing onset (Mikaelian et al., 1965; Sonntag et al., 2011). Synaptic function and structure change at this stage as the calyx of Held matures. The calyx undergoes a transformation from spoon-shaped to having many finger-like processes; this fenestration is associated with interdigitated astrocytes (Taschenberger et al., 2002; Ford et al., 2009). At this age, we found GFAP-positive fibrous processes that extended into both VCN and MNTB, while the cell bodies of these cells remained outside these auditory nuclei. Other astrocytic markers demonstrated similar staining to earlier ages. In addition, IBA1 staining revealed the presence of numerous microglia in VCN and MNTB. In our survey GFAP-positive fibers had highest expression in MNTB and VCN after hearing onset. Compared to the younger ages, OLIG2 expression appeared increased in VCN, but unchanged in MNTB. By P23, there was a decrease in GFAP expression, and ALDH1L1 staining appeared more punctate in MNTB. The change in appearance of ALDH1L1 expression coincides with the developmental age at which all the calyces have undergone a period of fenestration (Ford et al., 2009). In addition, the close apposition of ALDH1L1-positive astrocytes suggests that this particular astrocytic

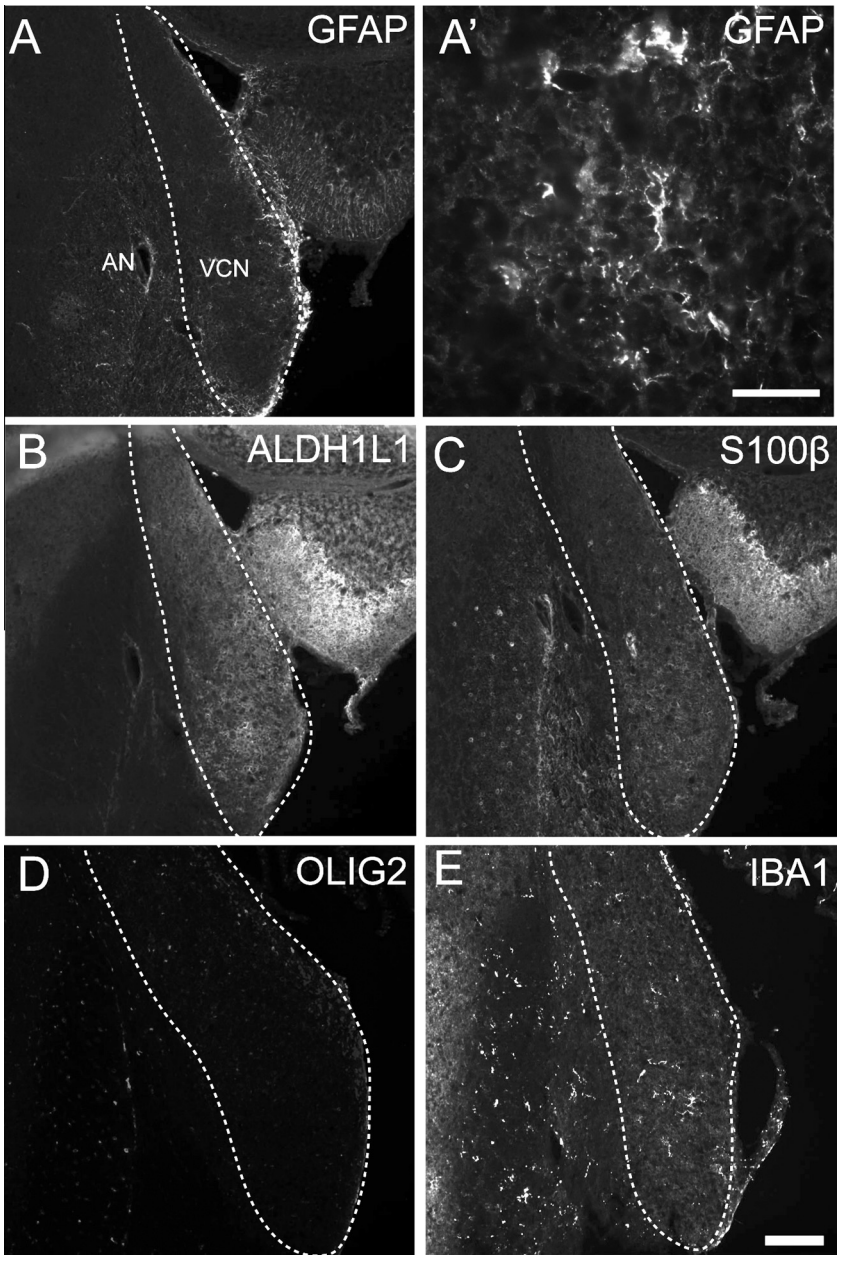

Fig. 7. Expression of glial markers in VCN at P23. (A) At P23, an increase in GFAP-positive fibers observed inside VCN with several processes (highlighted in A′ from a representative section). (B–C) Relatively low levels of expression were seen for S100β and ALDH1L1 surrounding VCN neurons. (D) VCN was populated with OLIG2-positive cells, (E) IBA1-positive cells were considerably less numerous than at earlier ages. Scale bar in E = 100 μm, applies to all panels except for A′, which has a Scale bar = 50 μm.

population may be important for the facilitation of glutamate uptake that is necessary for the calyx to have high fidelity synaptic transmission onto the principal neurons.

Oligodendrocytes expressed during brainstem development

We used an antibody that recognizes OLIG2, a known marker for embryonic, young, and mature oligodendrocytes (Takebayashi et al., 2000, 2002), to examine the developmental expression of oligodendrocytes. In all the ages we examined, oligodendrocytes were present throughout the brainstem, with more cells expressed at P14. Previously published studies using an alternate oligodendrocyte marker, myelin basic protein, have shown a similar expression pattern in rodent brainstem, of peak expression prior to adulthood (Delassalle et al., 1981; Foran and Peterson, 1992; Richardson et al., 2006). These observations suggest the presence of oligodendrocytes well in advance of myelination, which occurs in this pathway in rats after P8 (Leao et al., 2005).

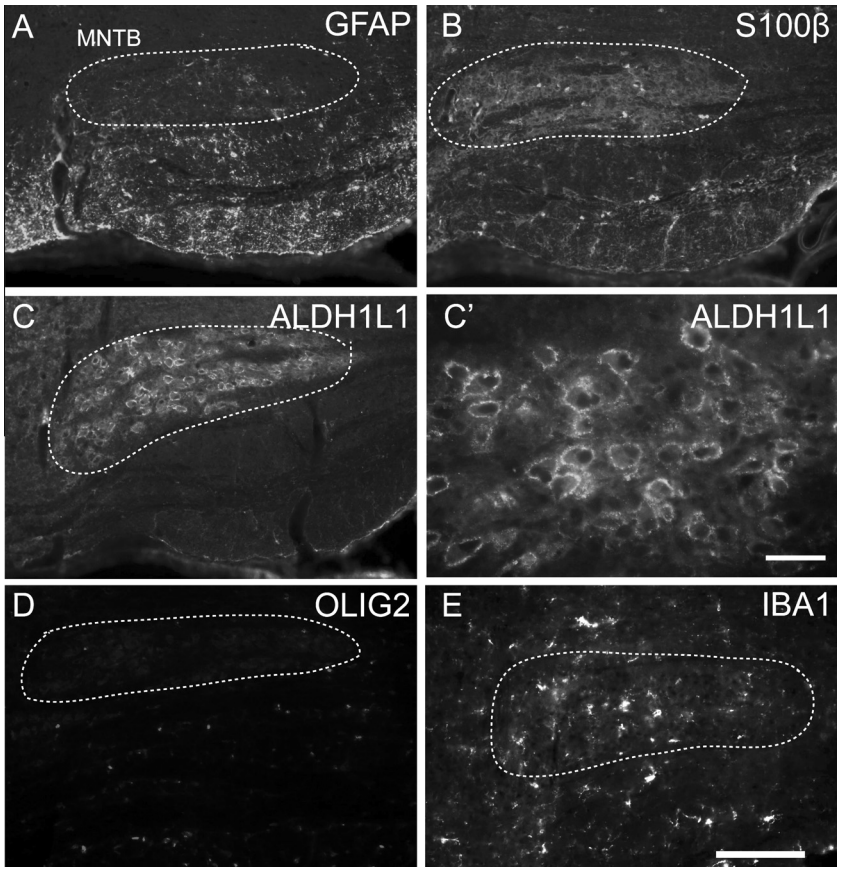

Fig. 8. Expression of glial markers in MNTB at P23. (A) At P23 there was significantly less GFAP-positive processes found in MNTB compared to at P14 ($p = 0.02$; GFAP at P23 was 368.97 ± 37.02 and GFAP at P14 was 821.08 ± 23.11). (B) S100β had low level of expression in brainstem. In contrast, many ALDH1L1-positive cells were surrounding individual MNTB principal neurons (C–C′). (D) OLIG2 expression was located ventral to MNTB. (E) IBA1-positive microglia were observed in a sparse distribution throughout MNTB. Scale bar in E = 100 μm, applies to all panels except panel C′ (Scale bar = 50 μm).

Temporally and spatially distinct classes of astrocytes

Our results suggest the presence of a heterogeneous population of astrocytes. Classically there are considered to be two astrocytic populations: fibrous and protoplasmic astrocytes. While fibrous astrocytes have more elongated processes and are largely located in white matter; protoplasmic astrocytes are more globular with fewer glial processes and are localized to gray matter (Miller and Raff, 1984). In our studies, we found that GFAP-expressing astrocytes appeared later in the brainstem compared to non-GFAP astrocytic markers, suggesting that distinct classes of astrocytes could have differing functions in brainstem development. In our study, GFAP-expressing astrocytes may represent the fibrous astrocytic population, as these astrocytes fit the criteria for having more elaborate processes and are found coursing along the VCN axon tracts to MNTB. In contrast, the morphology of ALDH1L1- and S100β-positive astrocytes was more consistent with protoplasmic astrocytic population; these cells are more rounded and while not found within the fiber tracts, are localized predominantly to the gray matter, surrounding the principal neurons. The early astrocytes are positioned to play a role in synaptogenesis. GFAP expression at later ages shows astrocytes in close apposition to the calyx of Held as well as localized to the VCN–MNTB fiber tracts, in parallel to studies done in the mature rat brain and cat visual cortex (Ghandour et al., 1980; Hajos and Kalman, 1989; Muller, 1992; Reyes-Haro et al., 2010). The localization of these cells is consistent with a possible role in regulating neurotransmission and/or facilitation of glutamatergic clearance (Renden et al., 2005; Reyes-Haro et al., 2010).

Delayed expression of GFAP-positive astrocytes and IBA1-positive microglia in MNTB

The early expression of the astrocyte markers ALDH1L1 and S100β contrasts with expression of GFAP in MNTB, which was not seen upregulated until after hearing onset. Minimal IBA1 expression was seen inside MNTB at P6. The appearance of GFAP-positive astrocytic fibers and IBA1-positive microglia within the MNTB occurs after formation of the calyx of Held, but during a time of maturation of the calyx (Ford et al., 2009; Borst and Soria van Hoeve, 2012). Our results are consistent with similar findings in chick auditory brainstem development, where GFAP-positive processes were observed entering the *n. laminaris* (NL) cell body layer late in

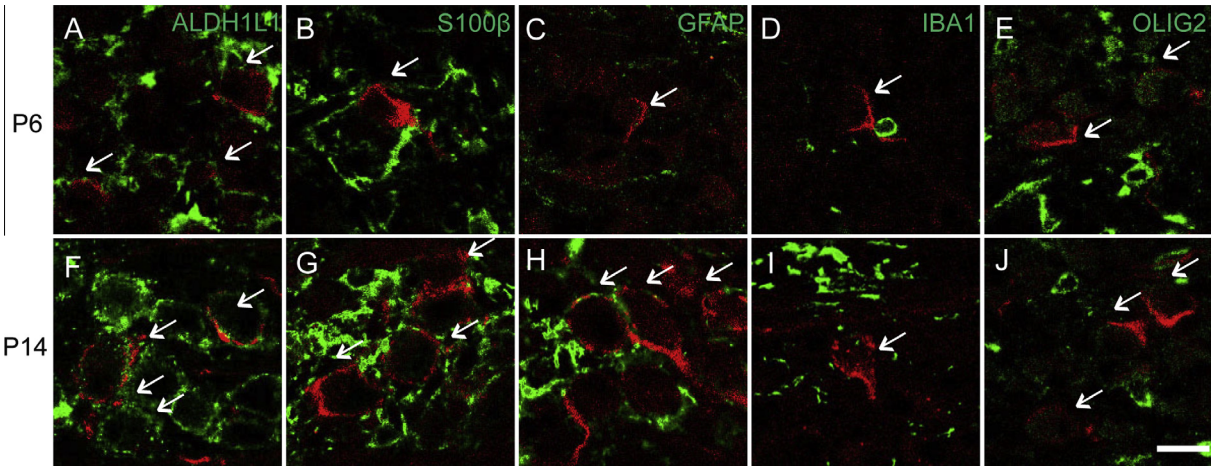

Fig. 9. Expression of glial markers in relation to the calyx at P6 and P14. (A-E) Glial cell types near P6 calyx. (A, B) Cells positive for ALDH1L1 and S100β were in close apposition to labeled calyces (calyces indicated with arrows). (C) Few GFAP-positive populations found within MNTB. (D) IBA1-positive cells were found scattered across MNTB, often close to the labeled calyx. (E) Oligodendrocytes fully surround postsynaptic neurons. (F–J) Glial cell types near P14 calyx. (F–G) All astrocytic markers found expressed close to developing calyx. ALDH1L1 and S100β-positive astrocytes were in close proximity to calyx and appeared to align closely to the MNTB neuron. (H) Several GFAP processes extended into MNTB and in some cases were seen in proximity to labeled calyces. (I) IBA1-positive cells were located near calyx and had larger cell bodies compared to younger age. (J) OLIG2-positive staining looked similar to younger age, often near the MNTB neuron. Scale bar in J = 25 μm; applies to all panels.

embryonic development (Korn and Cramer, 2008), at a time after formation of excitatory inputs to the nucleus (Saunders et al., 1973; Jackson and Parks, 1982; Young and Rubel, 1986). The delayed expression of GFAP in chick astrocytes coincides with dendritic reorganization of NL neurons and inhibitory synapse maturation. Furthermore, astrocyte-secreted factors were shown to mediate these developmental events using an *in vitro* preparation (Korn et al., 2011, 2012). The importance and identity of these factors will be of interest in the study of circuit formation in the mammalian auditory brainstem.

Morphological changes in microglia during postnatal brainstem development

IBA1 immunofluorescence showed that brainstem microglia undergo morphological changes early in postnatal development. At P0 we observed both ameboid microglial cells with no processes and cells with few processes emanating from the cell bodies. These microglia appeared more rounded, similar to previously described embryonic forms found in the rat hippocampus (Dalmau et al., 1997). IBA1 microglia observed at older postnatal ages were more dense and exhibited slightly ovoid cell bodies with complex, elongated radial processes, characteristic of the ramified forms observed during the second postnatal week of rat hippocampal development (Dalmau et al., 1998). At three postnatal weeks, microglia were numerous and demonstrated diversity of types, ranging from only cell bodies to cells with various processes (Lawson et al., 1990).

Distribution of astrocytes and microglia following unilateral CR

After unilateral CR during the early postnatal period, intact VCN axons branch and make aberrant connections with the denervated ipsilateral MNTB (Kitzes et al., 1995; Russell and Moore, 1995; Hsieh et al., 2007). Similar molecular cues limit ipsilateral projections both during normal development and after CR (Nakamura et al., 2012; Nakamura and Cramer, 2013). To further explore the similarities of these mechanisms, we examined the extent to which glial distributions in denervated MNTB resemble those seen during normal development. We found that CR was not associated with overall significant increases in glial cell density in MNTB compared to the unlesioned side. Nevertheless, astrocytic cells were closely localized to the newly developing ectopic calyx, similar to those seen in normal development. Both OLIG2-IBA1-positive cells were not preferentially located near nascent calyces, either during normal development or after unilateral lesion. The similarity in the spatial distribution of glial cells during developmental and induced synaptogenesis in MNTB is consistent with the view that these processes share molecular and cellular mechanisms.

A number of studies have shown increases in glial reactivity following deafferentation in the adult cochlear nucleus. An increase in astrocytes was found in chick brainstem after CR in *n. magnocellularis*, the avian homolog of the anteroventral cochlear nucleus (Rubel and MacDonald, 1992; Lurie and Rubel, 1994). Prior studies in mammals have also shown that both microglia and astrocytes are upregulated in the cochlear nucleus in response to unilateral inner ear lesions in adult rats (de Waele et al., 1996; Campos Torres et al., 1999; Campos-Torres et al., 2005; Fuentes-Santamaria et al., 2012). These studies showed changes in the cochlear nucleus, the primary target denervated by CR. In our studies, we explored changes in the MNTB, a secondary site of denervation. It is possible that changes in glial cell density are not reflected in this secondary site. Consistent with this possibility, unilateral CR did not alter proliferation in P9 rat MNTB (Saliu et al., 2014).

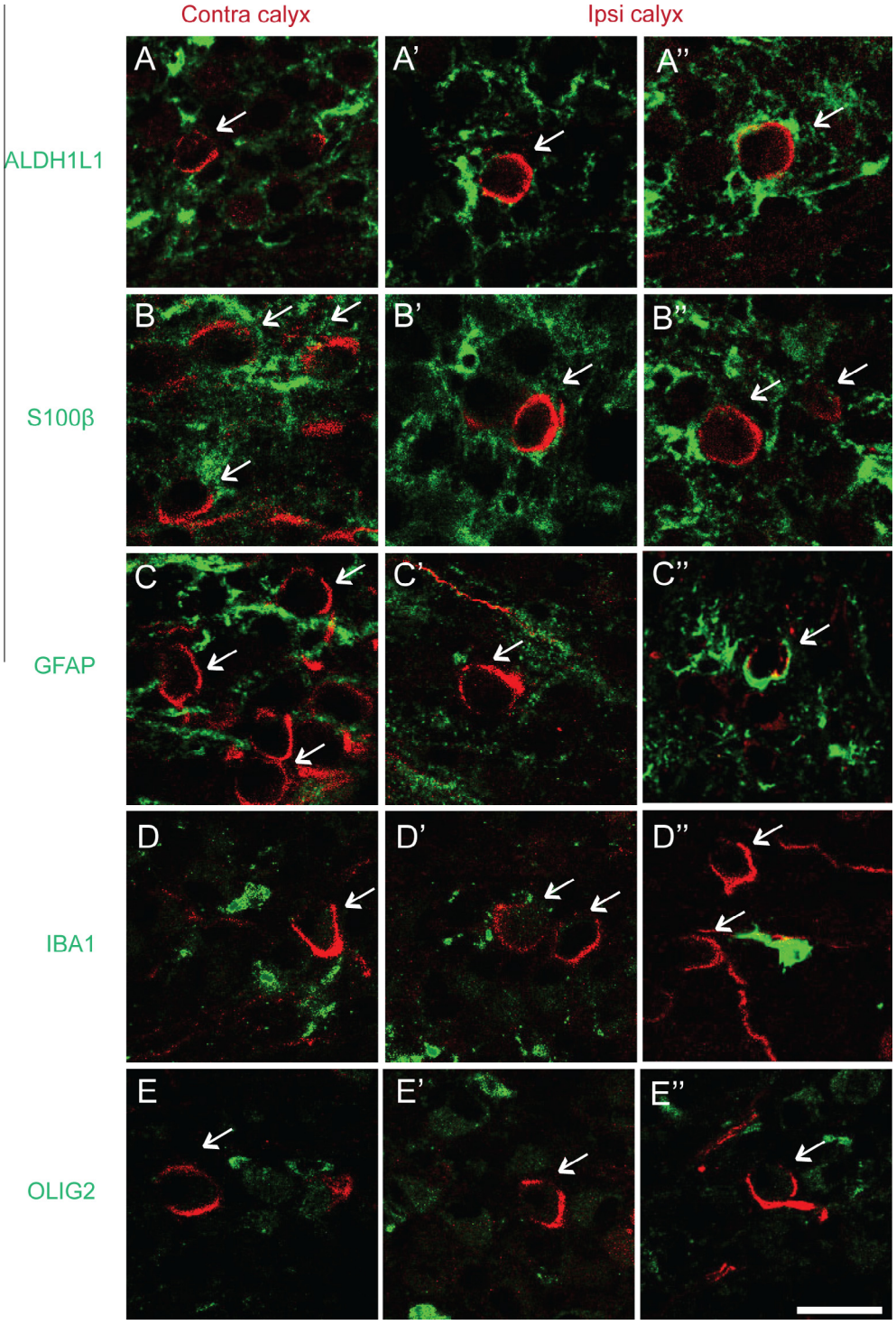

Fig. 10. Expression of glial markers in relation to ectopic calyx seven days following CR. (A) ALDH1L1-positive astrocytes located along postsynaptic space unoccupied by newly formed calyx, similar to contralateral calyx (calyces indicated with arrows). (B) S100β cells and processes situated around MNTB neurons in both contralateral and ectopic ipsilateral calyx. (C) Several GFAP-positive processes extended into MNTB region, with a majority of cells contacting both contralateral and ectopic calyces (example of close apposition in C″). (D) Unlike astrocytic populations, few microglia found near calyx. (E) Very few OLIG2-positive expression near calyces. Scale bar in E = 25 μm; applies to all panels.

Alternatively, it may be that changes in glial cell density require a longer time to emerge. Because we were interested in the formation of calyceal terminations, we limited our examination of glial markers to a time window after lesion when the new calyces form (Kitzes et al., 1995; Hsieh et al., 2007). Our findings suggest that glial cell configurations near induced projections are similar to those of normal projections, but that increases in glial number, through proliferation or migration, do not seem to be required for the induction of ipsilateral projections.

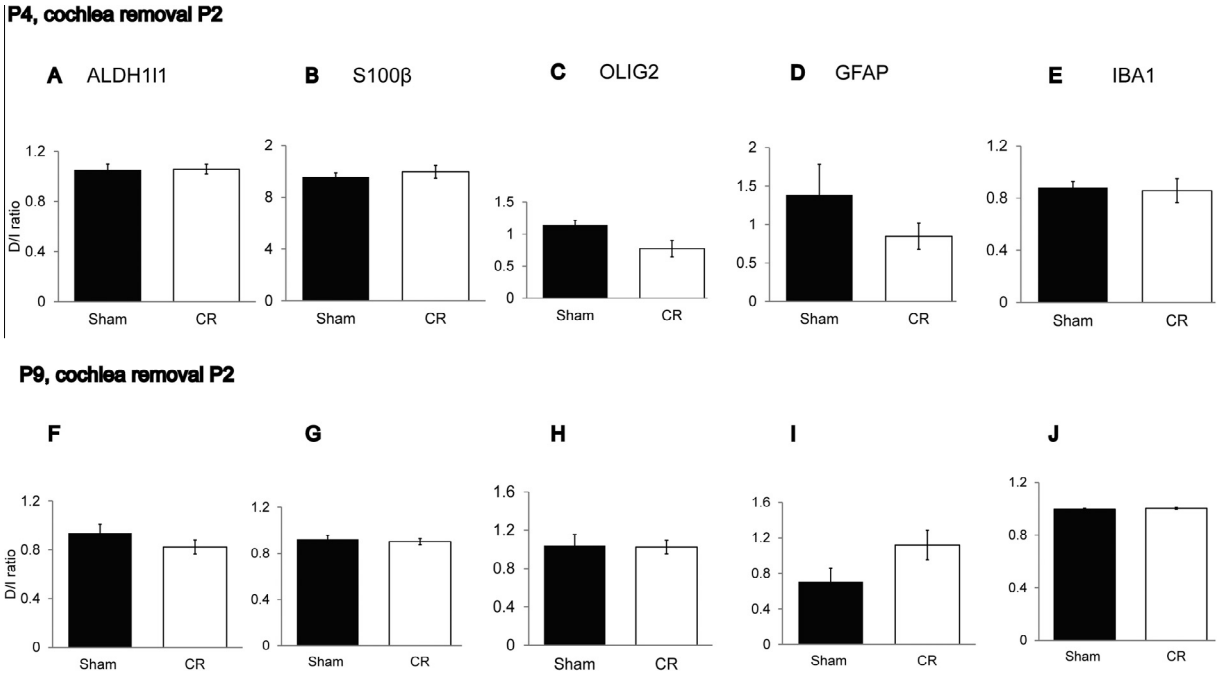

Fig. 11. Expression of glial markers two and seven days following unilateral CR. (A) No significant difference in expression pattern of glial markers two days after CR (ANOVA, $p = 0.23$). ALDH1L1 staining in CR animals had a mean D/I ratio of 1.06 ± 0.03 compared to sham animals (1.05 ± 0.05). (B) Expression of S100β cells for CR groups had a D/I ratio of 1.0 ± 0.05 compared to sham group (0.96 ± 0.03). (C) OLIG2 expression had a similar result when comparing CR groups to sham (1.14 ± 0.07 and 0.77 ± 0.13, respectively). (D) Number of GFAP-positive processes was not different – the CR group had a mean D/I ratio of 0.85 ± 0.15 processes compared to sham-operated animals, which had a D/I ratio of 1.38 ± 0.41. (E) Number of microglial cells comparing CR animals to sham was not significant (0.86 ± 0.09 compared to 0.88 ± 0.05). (F) One week after CR, no differences in glial marker distribution seen when comparing sham to CR groups (ANOVA, $p = 0.13$). Staining of ALDH1L1 showed that CR groups had a mean D/I ratio of 0.82 ± 0.06 and were not significantly different compared to the sham group (0.94 ± 0.07). (G) S100β expression between CR and sham was not different (0.9 ± 0.03 and 0.92 ± 0.03, respectively). (H) OLIG2 expression between CR and sham groups was not different with the CR group D/I ratio of 1.03 ± 0.07 and sham group D/I ratio of 1.04 ± 0.12. (I) When comparing GFAP processes, animals subjected to unilateral CR had a D/I ratio of 1.12 ± 0.17, a value greater than sham-operated animals but not significantly different (0.71 ± 0.15). (J) No change in between was seen in IBA1-positive cell density D/I ratio between CR and sham groups (1.0 ± 0.01 and 0.99 ± 0.01). Values are reported as mean ± SEM.

CONCLUSIONS

Our data show distinct expression profiles of glial markers in the developing mouse brainstem. We found that glial cells emerge early in development, during synaptogenesis of the VCN–MNTB circuit, and that these populations shift and change overtime. The results are consistent with a role for glial cells and their associated proteins in synapse formation and maturation in the auditory brainstem. Following CR, we found that the expression of glial markers after surgery was largely similar to that of normal development, with astrocytes surrounding both normal and lesion-induced calyces. These observations support the view that induction of new synapses after lesion relies on the same glial populations needed for normal development.

Acknowledgements—The authors are grateful to H. Nguyen and J. Ayala Salazar for technical support and to Dr. S. Cohen-Cory and Dr. K. Green for assistance with imaging. This work was supported by NIH T32 DC010775.

REFERENCES

Allen NJ, Bennett ML, Foo LC, Wang GX, Chakraborty C, Smith SJ, Barres BA (2012) Astrocyte glypicans 4 and 6 promote formation of excitatory synapses via GluA1 AMPA receptors. Nature 486:410–414.

Borst JG, Soria van Hoeve J (2012) The calyx of held synapse: from model synapse to auditory relay. Annu Rev Physiol 74:199–224.

Cahoy JD, Emery B, Kaushal A, Foo LC, Zamanian JL, Christopherson KS, Xing Y, Lubischer JL, Krieg PA, Krupenko SA, Thompson WJ, Barres BA (2008) A transcriptome database for astrocytes, neurons, and oligodendrocytes: a new resource for understanding brain development and function. J Neurosci 28:264–278.

Campos-Torres A, Touret M, Vidal PP, Barnum S, de Waele C (2005) The differential response of astrocytes within the vestibular and cochlear nuclei following unilateral labyrinthectomy or vestibular afferent activity blockade by transtympanic tetrodotoxin injection in the rat. Neuroscience 130:853–865.

Campos Torres A, Vidal PP, de Waele C (1999) Evidence for a microglial reaction within the vestibular and cochlear nuclei following inner ear lesion in the rat. Neuroscience 92:1475–1490.

Christopherson KS, Ullian EM, Stokes CC, Mullowney CE, Hell JW, Agah A, Lawler J, Mosher DF, Bornstein P, Barres BA (2005) Thrombospondins are astrocyte-secreted proteins that promote CNS synaptogenesis. Cell 120:421–433.

Chung WS, Barres BA (2012) The role of glial cells in synapse elimination. Curr Opin Neurobiol 22:438–445.

Dalmau I, Finsen B, Tonder N, Zimmer J, Gonzalez B, Castellano B (1997) Development of microglia in the prenatal rat hippocampus. J Comp Neurol 377:70–84.

Dalmau I, Finsen B, Zimmer J, Gonzalez B, Castellano B (1998) Development of microglia in the postnatal rat hippocampus. Hippocampus 8:458–474.

de Waele C, Campos Torres A, Josset P, Vidal PP (1996) Evidence for reactive astrocytes in rat vestibular and cochlear nuclei following unilateral inner ear lesion. Eur J Neurosci 8: 2006–2018.

Delassalle A, Zalc B, Lachapelle F, Raoul M, Collier P, Jacque C (1981) Regional distribution of myelin basic protein in the central nervous system of quaking, jimpy, and normal mice during development and aging. J Neurosci Res 6:303–313.

Elezgarai I, Bilbao A, Mateos JM, Azkue JJ, Benitez R, Osorio A, Diez J, Puente N, Donate-Oliver F, Grandes P (2001) Group II metabotropic glutamate receptors are differentially expressed in the medial nucleus of the trapezoid body in the developing and adult rat. Neuroscience 104:487–498.

Foran DR, Peterson AC (1992) Myelin acquisition in the central nervous system of the mouse revealed by an MBP-Lac Z transgene. J Neurosci 12:4890–4897.

Ford MC, Grothe B, Klug A (2009) Fenestration of the calyx of Held occurs sequentially along the tonotopic axis, is influenced by afferent activity, and facilitates glutamate clearance. J Comp Neurol 514:92–106.

Fuentes-Santamaria V, Alvarado JC, Juiz JM (2012) Long-term interaction between microglial cells and cochlear nucleus neurons after bilateral cochlear ablation. J Comp Neurol 520:2974–2990.

Ghandour MS, Vincendon G, Gombos G (1980) Astrocyte and oligodendrocyte distribution in adult rat cerebellum: an immunohistological study. J Neurocytol 9:637–646.

Hajos F, Kalman M (1989) Distribution of glial fibrillary acidic protein (GFAP)-immunoreactive astrocytes in the rat brain. II. Mesencephalon, rhombencephalon and spinal cord. Exp Brain Res 78:164–173.

Hashisaki GT, Rubel EW (1989) Effects of unilateral cochlea removal on anteroventral cochlear nucleus neurons in developing gerbils. J Comp Neurol 283:5–73.

Hoffpauir BK, Grimes JL, Mathers PH, Spirou GA (2006) Synaptogenesis of the calyx of Held: rapid onset of function and one-to-one morphological innervation. J Neurosci 26: 5511–5523.

Holcomb PS, Hoffpauir BK, Hoyson MC, Jackson DR, Deerinck TJ, Marrs GS, Dehoff M, Wu J, Ellisman MH, Spirou GA (2013) Synaptic inputs compete during rapid formation of the calyx of Held: a new model system for neural development. J Neurosci 33:12954–12969.

Hsieh CY, Cramer KS (2006) Deafferentation induces novel axonal projections in the auditory brainstem after hearing onset. J Comp Neurol 497:589–599.

Hsieh CY, Hong CT, Cramer KS (2007) Deletion of EphA4 enhances deafferentation-induced ipsilateral sprouting in auditory brainstem projections. J Comp Neurol 504:508–518.

Hughes EG, Elmariah SB, Balice-Gordon RJ (2010) Astrocyte secreted proteins selectively increase hippocampal GABAergic axon length, branching, and synaptogenesis. Mol Cell Neurosci 43:136–145.

Jackson H, Parks TN (1982) Functional synapse elimination in the developing avian cochlear nucleus with simultaneous reduction in cochlear nerve axon branching. J Neurosci 2:1736–1743.

Kandler K, Friauf E (1993) Pre- and postnatal development of efferent connections of the cochlear nucleus in the rat. J Comp Neurol 328:161–184.

Karimi-Abdolrezaee S, Billakanti R (2012) Reactive astrogliosis after spinal cord injury-beneficial and detrimental effects. Mol Neurobiol 46:251–264.

Kil J, Kageyama GH, Semple MN, Kitzes LM (1995) Development of ventral cochlear nucleus projections to the superior olivary complex in gerbil. J Comp Neurol 353:317–340.

Kitzes LM, Kageyama GH, Semple MN, Kil J (1995) Development of ectopic projections from the ventral cochlear nucleus to the superior olivary complex induced by neonatal ablation of the contralateral cochlea. J Comp Neurol 353:341–363.

Korn MJ, Cramer KS (2008) Distribution of glial-associated proteins in the developing chick auditory brainstem. Dev Neurobiol 68:1093–1106.

Korn MJ, Koppel SJ, Cramer KS (2011) Astrocyte-secreted factors modulate a gradient of primary dendritic arbors in nucleus laminaris of the avian auditory brainstem. PLoS One 6:e27383.

Korn MJ, Koppel SJ, Li LH, Mehta D, Mehta SB, Seidl AH, Cramer KS (2012) Astrocyte-secreted factors modulate the developmental distribution of inhibitory synapses in nucleus laminaris of the avian auditory brainstem. J Comp Neurol 520:1262–1277.

Kucukdereli H, Allen NJ, Lee AT, Feng A, Ozlu MI, Conatser LM, Chakraborty C, Workman G, Weaver M, Sage EH, Barres BA, Eroglu C (2011) Control of excitatory CNS synaptogenesis by astrocyte-secreted proteins Hevin and SPARC. Proc Natl Acad Sci U S A 108:E440–E449.

Kuwabara N, DiCaprio RA, Zook JM (1991) Afferents to the medial nucleus of the trapezoid body and their collateral projections. J Comp Neurol 314:684–706.

Kuwabara N, Zook JM (1991) Classification of the principal cells of the medial nucleus of the trapezoid body. J Comp Neurol 314:707–720.

Lawson LJ, Perry VH, Dri P, Gordon S (1990) Heterogeneity in the distribution and morphology of microglia in the normal adult mouse brain. Neuroscience 39:151–170.

Leao RM, Kushmerick C, Pinaud R, Renden R, Li GL, Taschenberger H, Spirou G, Levinson SR, von Gersdorff H (2005) Presynaptic Na+ channels: locus, development, and recovery from inactivation at a high-fidelity synapse. J Neurosci 25:3724–3738.

Lurie DI, Rubel EW (1994) Astrocyte proliferation in the chick auditory brainstem following cochlea removal. J Comp Neurol 346:276–288.

Mauch DH, Nagler K, Schumacher S, Goritz C, Muller EC, Otto A, Pfrieger FW (2001) CNS synaptogenesis promoted by glia-derived cholesterol. Science (New York, NY) 294:1354–1357.

Mikaelian D, Alford BR, Ruben RJ (1965) Cochlear potentials and 8 nerve action potentials in normal and genetically deaf mice. Ann Otol Rhinol Laryngol 74:146–157.

Miller RH, Raff MC (1984) Fibrous and protoplasmic astrocytes are biochemically and developmentally distinct. J Neurosci 4:585–592.

Moore DR, Kowalchuk NE (1988) Auditory brainstem of the ferret: effects of unilateral cochlear lesions on cochlear nucleus volume and projections to the inferior colliculus. J Comp Neurol 272:503–515.

Mostafapour SP, Cochran SL, Del Puerto NM, Rubel EW (2000) Patterns of cell death in mouse anteroventral cochlear nucleus neurons after unilateral cochlea removal. J Comp Neurol 426:561–571.

Muller CM (1992) Astrocytes in cat visual cortex studied by GFAP and S-100 immunocytochemistry during postnatal development. J Comp Neurol 317:309–323.

Nakamura PA, Cramer KS (2011) Formation and maturation of the calyx of Held. Hear Res 276:70–78.

Nakamura PA, Cramer KS (2013) EphB2 signaling regulates lesion-induced axon sprouting but not critical period length in the postnatal auditory brainstem. Neural Dev 8:2.

Nakamura PA, Hsieh CY, Cramer KS (2012) EphB signaling regulates target innervation in the developing and deafferented auditory brainstem. Dev Neurobiol 72:1243–1255.

Renden R, Taschenberger H, Puente N, Rusakov DA, Duvoisin R, Wang LY, Lehre KP, von Gersdorff H (2005) Glutamate transporter studies reveal the pruning of metabotropic glutamate receptors and absence of AMPA receptor desensitization at mature calyx of held synapses. J Neurosci 25:8482–8497.

Reyes-Haro D, Muller J, Boresch M, Pivneva T, Benedetti B, Scheller A, Nolte C, Kettenmann H (2010) Neuron-astrocyte interactions in the medial nucleus of the trapezoid body. J Gen Physiol 135:583–594.

Richardson WD, Kessaris N, Pringle N (2006) Oligodendrocyte wars. Nat Rev Neurosci 7:11–18.

Rodriguez-Contreras A, van Hoeve JS, Habets RL, Locher H, Borst JG (2008) Dynamic development of the calyx of Held synapse. Proc Natl Acad Sci U S A 105:5603–5608.

Rubel EW, MacDonald GH (1992) Rapid growth of astrocytic processes in N. magnocellularis following cochlea removal. J Comp Neurol 318:415–425.

Russell FA, Moore DR (1995) Afferent reorganisation within the superior olivary complex of the gerbil: development and induction by neonatal, unilateral cochlear removal. J Comp Neurol 352:607–625.

Saliu A, Adise S, Xian S, Kudelska K, Rodriguez-Contreras A (2014) Natural and lesion-induced decrease in cell proliferation in the medial nucleus of the trapezoid body during hearing development. J Comp Neurol 522:Spc1.

Saunders JC, Coles RB, Gates GR (1973) The development of auditory evoked responses in the cochlea and cochlear nuclei of the chick. Brain Res 63:59–74.

Schafer DP, Lehrman EK, Kautzman AG, Koyama R, Mardinly AR, Yamasaki R, Ransohoff RM, Greenberg ME, Barres BA, Stevens B (2012) Microglia sculpt postnatal neural circuits in an activity and complement-dependent manner. Neuron 74:691–705.

Sonntag M, Englitz B, Typlt M, Rubsamen R (2011) The calyx of held develops adult-like dynamics and reliability by hearing onset in the mouse in vivo. J Neurosci 31:6699–6709.

Takebayashi H, Nabeshima Y, Yoshida S, Chisaka O, Ikenaka K (2002) The basic helix-loop-helix factor olig2 is essential for the development of motoneuron and oligodendrocyte lineages. Curr Biol: CB 12:1157–1163.

Takebayashi H, Yoshida S, Sugimori M, Kosako H, Kominami R, Nakafuku M, Nabeshima Y (2000) Dynamic expression of basic helix-loop-helix Olig family members: implication of Olig2 in neuron and oligodendrocyte differentiation and identification of a new member, Olig3. Mech Dev 99:143–148.

Taschenberger H, Leao RM, Rowland KC, Spirou GA, von Gersdorff H (2002) Optimizing synaptic architecture and efficiency for high-frequency transmission. Neuron 36:1127–1143.

Trune DR (1982) Influence of neonatal cochlear removal on the development of mouse cochlear nucleus: I. Number, size, and density of its neurons. J Comp Neurol 209:409–424.

Wake H, Moorhouse AJ, Miyamoto A, Nabekura J (2013) Microglia: actively surveying and shaping neuronal circuit structure and function. Trends Neurosci 36:209–217.

Young SR, Rubel EW (1986) Embryogenesis of arborization pattern and topography of individual axons in *N. laminaris* of the chicken brain stem. J Comp Neurol 254:425–459.

(Accepted 15 August 2014)
(Available online 24 August 2014)